Springer

KSME

Journal of Mechanical Science and Technology 26 (6) (2012) 1747~1752
www.springerlink.com/content/1738-494x
DOI 10.1007/s12206-012-0340-8

Fatigue life analysis of shot-peened bearing steel †

Sang-Jae Yoon[1], Jung-Hoon Park[1] and Nak-Sam Choi[2,*]

[1]*Department of Mechanical Engineering, Graduate School, Hanyang University, 222Wangsimni-ro, Seongdong-gu, Seoul 133-791, Korea*
[2]*Department of Mechanical Engineering, Hanyang University, 55Hanyangdaehak-ro, Sangnok-gu, Ansan 426-791, Korea*

(Manuscript Received August 20, 2011; Revised January 12, 2012; Accepted January 12, 2012)

Abstract

Shot-peening effects on the fatigue life behavior of bearing steel (JIS SUJ2) have been investigated. Hourglass-shaped test specimens were heat-treated and then surface-treated using a shot-peening machine. Results of a rotary bending fatigue test showed that shot-peening suppressed not only much of the surface-originated fracture but also the scattering error of the probabilistic stress-life data, and improved the fatigue life by about 6 times through the load levels of the cyclic tests. Such large increase in fatigue life was driven by the following reasons: The increase of hardness in the skin caused the predicted fatigue limit stress to increase by 15%; fracture-initiating inclusions were distributed at deeper locations, experiencing low nominal stresses; and the increase in the fish-eye fracture size by an average of 180%.

Keywords: Bearing steel; Bending fatigue test; Probabilistic–stress-life; Fish-eye fracture; Shot-peening

1. Introduction

Shot-peening treatments have been one of the excellent and economic methods being applied for the fatigue life enhancement of high strength steels [1]. Shiozawa et al. [2] reported the shot-peening effects in delaying the crack initiation and propagation over the giga-cycle fatigue life range of high carbon chromium steel. Cheng et al. [3] studied the fatigue strength behaviors influenced by the sizes, velocities and striking angles of shot steel balls. Many other studies [4, 5] have been performed on the fatigue resistances of a variety of steels treated with shot-peening processes. Most of the fatigue fractures originated from inclusions of small oxide particles or grain boundaries in the metal, forming a distinct zone called the "fish-eye region" on the fracture surface. This region is a small, optically bright spot that surrounds the crack origin on the fracture surface that is commonly observed for hardened steels. The fatigue life should depend on the depths of fracture initiation sites, and thus on the amount of the nominal stress at the sites that are located on the surface and/or in the interior as Murakami mentioned [6]. However, previous fatigue studies for shot-peened high strength steels have scarcely considered statistical aspects in the life test data and the fish-eye fracture feature.

In this study, shot-peening effects were statistically examined in the rotary bending fatigue test data of bearing steel. The fatigue life data was analyzed in association with skin hardness, nominal stress and fish-eye fracture region geometry.

*Corresponding author. Tel.: +82 400 5283, Fax.: +82 406 7063
E-mail address: nschoi@hanyang.ac.kr
† Recommended by Editor Jai Hak Park

2. Materials and methods

2.1 Materials and treatments

A high strength bearing steel (JIS-SUJ2) often employed for power transmission components in vehicles was used in this study. The chemical composition was C (0.99 wt%), Si (0.25), Mn (0.30), P (0.013), S (0.005), Cr (1.45), Cu (0.10), and Ni (0.06). Hourglass-shaped specimens with a gage portion 30mm in length and 6mm in diameter as shown in Fig. 1 were made according to the JIS Z 2274 standard [7]. The specimens were heated at 830℃ for 40 minutes and tempered at 160℃ for 40 minutes, and then cooled in air. A shot-peening treatment employing an impeller type shot-peening machine with an impeller diameter of 360 mm was conducted following the condition widely used in industry: Shot steel balls 0.3 mm in diameter impacted all the specimen surfaces for 6 minutes. The surface coverage by the shot-peening was about 300%.

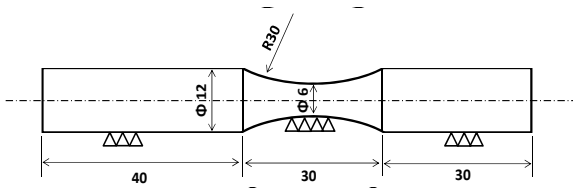

Fig. 1. Geometry of hourglass-shaped test specimen (unit: mm).

2.2 Residual stress measurement and rotary bending fatigue test

The residual stress in the specimen skin part was measured with the $2\theta - \sin^2\psi$ method [8] using an X-ray diffractometer (XStress3000), where ψ is an X-ray incidence angle, and θ is an X-ray diffraction angle in the material. The residual stress was measured with repeated electrolytic polishing from the surface to a depth 120 μm at an interval of 2μm.Vickers hardness was also measured at ten different locations on the surface. The ultimate static load of the specimens with a geometry shown in Fig. 1 was measured using a tensile tester (MTS-25 ton) with a displacement rate of 1 mm/min. A four-point type rotary bending fatigue tester (SHIMADZU, H7) was used for the fatigue test of the specimens. The load ratio (R) was maintained at -1 and the rotating speed was 3000 rpm. Four load levels and five specimens at each load level were chosen: the maximum load levels of the gage part were adjusted to levels of 38%, 42%, 46% and 50% of the ultimate static load (about 2543 MPa) measured in the tensile test, which conformed to KS B ISO 1143 standards [9].

The nominal tensile stress σ in the specimen is

$$\sigma = \frac{Mc}{I} \tag{1}$$

where M is the maximum bending moment ($= P \times m/2$), c is the distance from the neutral axis to a designated height in the specimen, I is the geometrical moment of inertia at the gage part ($= \pi d^4/64$). P, m and d are the load, the fixed test span (30 mm) and the gage part cross-section diameter (6 mm) of the specimen, respectively. After the fatigue tests, the fracture surface was analyzed by a scanning electron microscopy (SEM) and a dispersive X-ray spectroscopy (EDX).

3. Results and discussion

3.1 Shot-peening effects on residual stress, hardness and tensile strength

Residual stress distributions along the depth of the specimens are shown in Fig. 2. The skin of the shot-peened specimen contained the maximum compressive residual stress of about-1530 MPa that was about 3.7 times higher than that (-418 MPa) of the non-shot-peened one. The compressive stresses were distributed from the surface to a depth of about 90 μm. The Vickers hardness of 1019 ± 10Hv measured for the shot-peened specimens was 1.18 times as large as that for the non-shot-peened ones. The considerable increase in hardness indicates that the shot-peening brought into locally strengthened and thus hardened surfaces in the specimens. The ultimate tensile strength was improved by 0.3% on average, suggesting that the shot-peening effects were limited to a thin surface skin layer as in the above residual stress distribution.

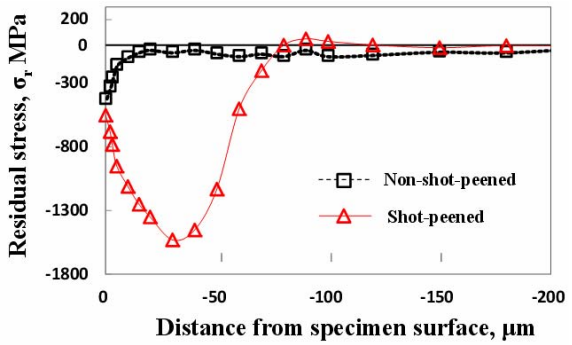

Fig. 2. Residual stress distribution in the shot-peened specimen.

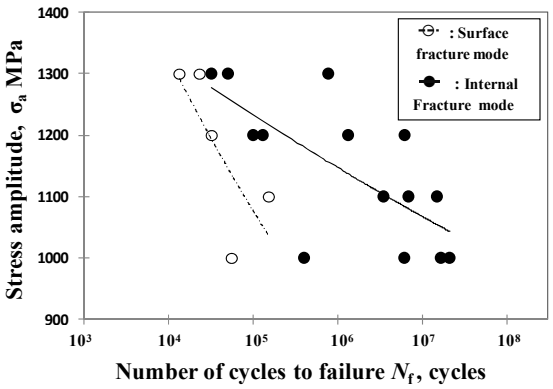

(a)

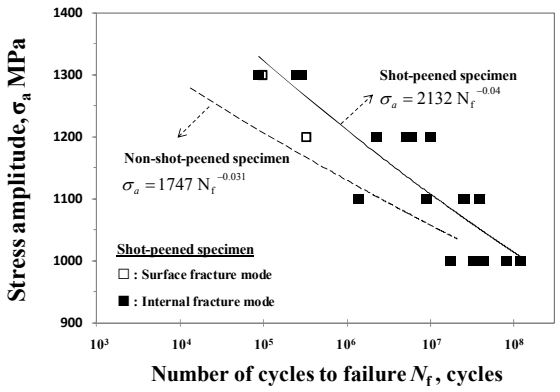

(b)

Fig. 3. The S–N curves of bearing steel: (a) non-shot-peened specimen; (b) shot-peened specimen.

3.2 Shot-peening effects on the probabilistic stress-life behavior

Fig. 3 shows test data points of the stress amplitude levels (S) and the corresponding cycles-to-failure (N) for non-shot-peened and shot-peened bearing steel specimens. The fatigue life of shot-peened specimens at each stress level was largely improved: the fatigue life was 6.7 times on average longer than that of non-shot-peened specimens. The life data obtained from the internal fractures were much longer than those from

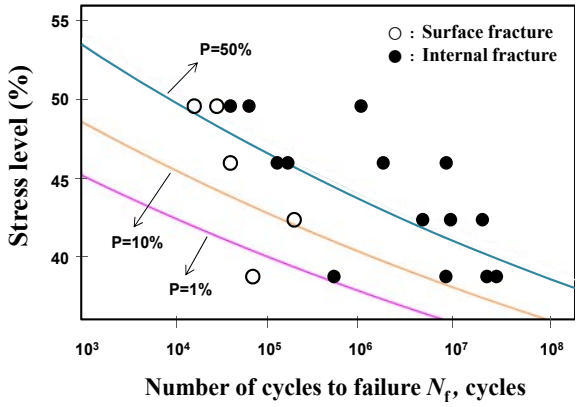

(a)

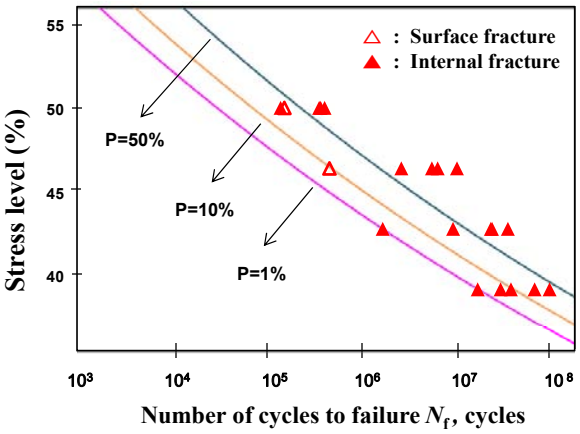

(b)

Fig. 4. Probability-stress-life (P-S-N) curves: (a) non-shot-peened specimen; (b) shot-peened specimen.

the surface fracture. Simple linear regression of the test data of log S versus log N using the least square calculation made an average prediction equation for each kind of the specimen as expressed in Fig. 3(b).

Because the life data at each load level in bearing steel may fit with Weibull distributions as mentioned in Ref. [10], probability-stress-life (P-S-N) curves were calculated using the maximum likelihood approach based on 2-parameter Weibull distributions. A P-S-N curve with the allowable life x_{ai} at each stress level S_i can be represented by the following equation [11]:

$$\log x_{ai} = -b \log S_i - \log K \tag{2}$$

where K and b are material coefficients. Using probability coefficients with a confidence level of 95%, values of K and b can be calculated with the least square method. According to the failure probabilities (p) of 1%, 10% and 50%, P-S-N curves for non-shot-peened and shot-peened specimens were obtained through Eq. (2) as shown in Fig. 4(a) and (b), respectively. At a constant failure probability the stress level at the allowable life was much up-graded by the shot-peening. Because the slope b = 27.0 was much lower than that (37.0) for non-shot-peened ones, the fatigue life improvement by the shot-peening diminished with decreasing the stress level, as similarly reported by Shiozawa et al. [2].

Table 1. Sum of squared error (SSE) values between fatigue life results and P-S-N curve.

Sum of squared error (SSE) value	Non-shot-peened specimen	Shot-peened specimen
*SSE**	14.86	4.78
*SSE***	151.80	19.73

$$\mathrm{SSE}^{*} = \sum_{i=1}^{4}\sum_{j=1}^{5}(\log x_{ij} - \log x_{i(p=50)})^2 \tag{3}$$

$$SSE^{**} = \sum_{i=1}^{4}\sum_{j=1}^{5}(\log x_{ij} - \log x_{i(p=1)})^2 \tag{4}$$

Such large scattering in the fatigue life test data of non-shot-peened specimens seemed to have been caused by various geometries and positions of oxide particle inclusions at fracture initiation sites. Because the shot-peening brought about locally strengthened surface skins having large compressive stresses as described above, the fracture initiation on the surface and in the skin layer was greatly suppressed. The probabilities of the surface fractured specimens were 25% in non-shot-peened ones, and 10% in shot-peened ones (compare Figs. 3(a) and 3(b)). Most of the fractures for shot-peened ones originated from the inclusions in the interior underneath the strengthened skin layer, which will be considered further in Section 3.3. Moreover, the suppression of the surface fracture led to a great reduction of the scattering amount of life data.

The scattering amount of the individual data from the average log N at each stress level can be analyzed for reliability evaluation of the life test data. The sum of squared error (SSE*) between the logarithmic life test data, $\log x_{ij}$, and the corresponding life estimation values at p = 50%, $\log x_{i(p=50)}$, can be calculated with Eq. (3).

Another case (SSE**) of the sum of squared error can be calculated on Eq. (4). In contrast with the highly scattered life test data of non-shot-peened specimens, SSE* and SSE** calculated for shot-peened ones greatly reduced to 32% and 13% of the non-shot-peened results, respectively (see Table 1). SSE** was much more sensitive to the shot-peening effects than SSE*. Thus, the scattering amount of the individual data from the average log N at each stress level was greatly reduced for shot-peened ones, which represents much reliable life. The P-S-N curves are representative of quantitative characteristics in the fatigue life at a given failure probability, and can be used for the reliable determination of the life corresponding to each stress level.

3.3 Quantitative analysis of the fish-eye region

As shown in Fig. 3, the fatigue life of the internal fracture

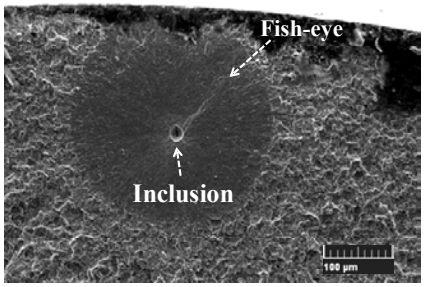

(a)

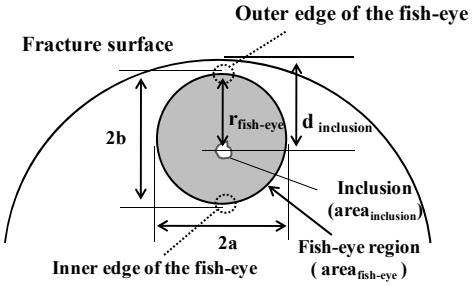

(b)

Fig. 5. (a) SEM observation of the fracture surface; (b) definition of internal crack geometrical parameter.

was much longer than that of the surface fracture. The surface fracture propagated rapidly after the initiation on the specimen surface. However, the internal fracture formed a 'fish-eye' region in the course of the initial slow crack growth. The typical fatigue fracture surface formed by a fracture initiation in the specimen interior and its schematic illustration are shown in Fig. 5(a) and (b), respectively. An alumina oxide particle was observed at the origin of the fish-eye fracture as examined by the EDX analysis. Such hard inclusion induced a stress concentration to initiate the fatigue fracture. The shape of a fish-eye was affected by the stress distribution in the vicinity of the inclusion. Because in the rotary bending fatigue test the stress gradient became higher in the side of the surface skin, the outer edge side of the fish-eye was a bit more grown than the inner edge. Several researchers [13, 14] reported similar behaviors of the fish-eye shape (2a, 2b), depending on the loading type and the loading rate in the rotary fatigue tests. The present study measured the area of the fish-eye region ($area_F$) for each test specimen.

Fig. 6 shows the behaviors of the fish-eye size $\sqrt{area_F}$ according to the levels of stress amplitude. The lowest value of $\sqrt{area_F}$ for the shot-peened specimens obviously jumped up in comparison to the non-shot-peened case. At the respective stress levels the mean value of $\sqrt{area_F}$ was larger by about 180% on average. As the stress level decreased, the average $\sqrt{area_F}$ increased considerably, whereas the non-shot-peened specimens showed an increasing trend in the data of $\sqrt{area_F}$ but a wide scattering band. The large increase of $\sqrt{area_F}$ for the shot-peened specimens brought about such a big increase of the fatigue life as shown in Fig. 7.

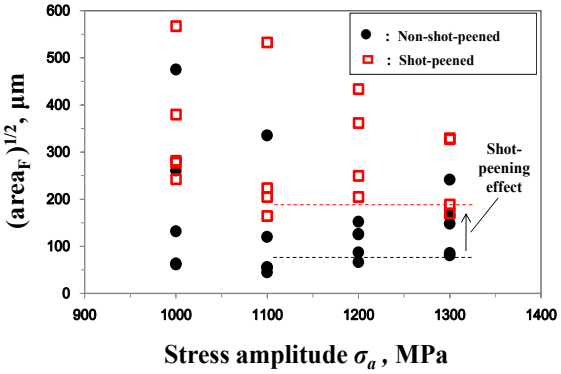

Fig. 6. Relationship between fish-eye size and stress amplitude.

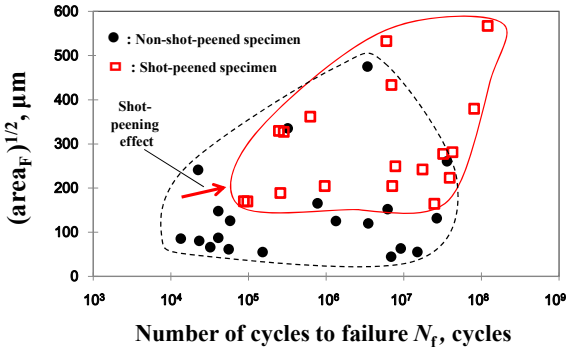

Fig. 7. Relationship between fish-eye size and N_f.

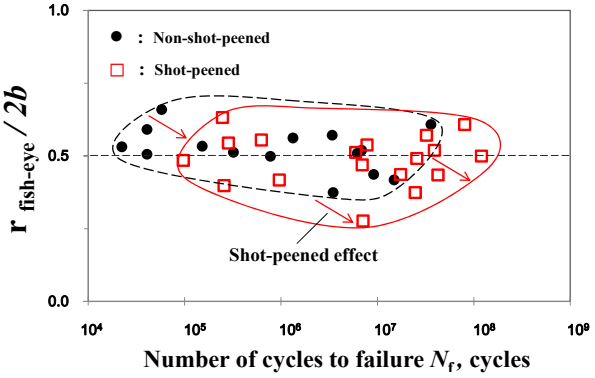

Fig. 8. Relationship between $r_{fish\text{-}eye}/2b$ and N_f.

Furthermore, the shot-peening caused values of $r_{fish\text{-}eye}$ /2b to be lower than those for non-shot-peened ones, making 70% of the values even lower than 0.5 as shown in Fig. 8, where $r_{fish\text{-}eye}$ was the outer radius of the fish-eye region illustrated in Fig. 5(b). Although the higher normal stress was applied to the outer edge than the inner edge of the fish-eye fracture in the rotary bending fatigue tests, this phenomenon was because the hardening and the compressive residual stress in the skin layer stated in Section 3.1 suppressed the initial crack growth from the inclusion toward the surface, causing the increase of the fish-eye area by about 180% on average as stated above [12].

A fatigue limit stress σ_w may be predicted with the equation

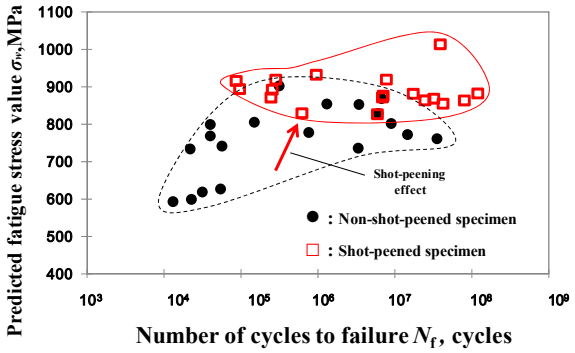

Fig. 9. Relationship between σ_w and N_f.

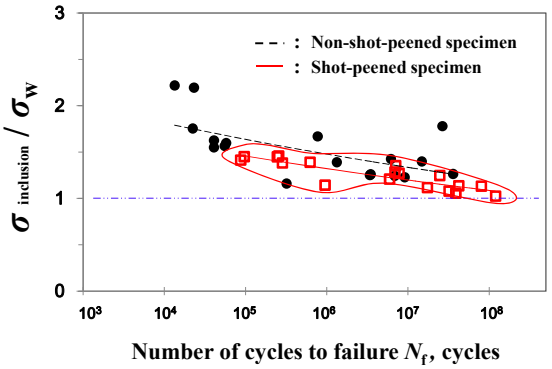

Fig. 10. Relationship between $\sigma_{inclusion}$ / σ_w and N_f.

$$\sigma_w \approx e(\mathrm{Hv}+120)/(\sqrt{\mathrm{area}_{\mathrm{inclusion}}})^{1/6} \quad (5)$$

where e is 1.43 and 1.56 for surface and internal fractures, respectively [6]. Fig. 9 shows behaviors of σ_w versus N_f. The average value of σ_w for shot-peened ones was on a higher level by 15% than that for non-shot-peened ones, implying a higher fatigue strength and a longer fatigue life at an identical bending load. On the other hand, a fracture can initiate at an inclusion when the nominal stress $\sigma_{inclusion}$calculated by Eq. (1) at the location of the inclusion exceeds σ_w. As shown in Fig. 10, $\sigma_{inclusion}$/ σ_w was higher than 1.0 in the present test data, indicating that the fatigue fracture arose for all the test specimens. The low $\sigma_{inclusion}$/ σ_w for shot-peened ones represents a fracture-initiating inclusion positioned at deeper location from the surface and thus a longer fatigue life as compared with non-shot-peened cases.

4. Conclusions

The rotary bending fatigue test was carried out using the shot-peened high strength bearing steel (JIS-SUJ2). The shot-peening hardened the skin and formed the compressive residual stress in the skin, suppressing much the scattering error of the probabilistic stress-life data and improving the average fatigue life by 6.7 times. The increase of the predicted fatigue limit stress, the decrease in the nominal stress around the fracture-initiating inclusion and the increase in the fish-eye fracture size brought about the large life improvement.

Nomenclature

ψ	: X-ray incidence angle
θ	: X-ray diffraction angle in the material
R	: Load ratio
σ	: Nominal tensile stress
M	: Maximum bending moment
c	: Distance from the neutral axis to a designated height in the specimen
I	: Geometrical moment of inertia at the gage part
P	: Load
m	: Fixed test span
d	: Gage part cross-section diameter of the specimen
Hv	: Vickers hardness
x_{ai}	: Allowable life
S_i	: Stress level
K	: Material coefficient
b	: Material coefficient
$\log x_{ai}$	: Logarithmic life test data
$r_{fish\text{-}eye}$	: Outer radius of the fish-eye region
σ_w	: Fatigue limit stress
e	: Material coefficient

References

[1] P. Zhang and J. Lindemann, Influence of shot peening on high cycle fatigue properties of the high-strength wrought magnesium alloy AZ80, *Scripta Materialia,* 52 (6) (2005) 485-490.

[2] K. Shiozawa and L. Lu, Very high-cycle fatigue behaviour of shot-peened high-carbon-chromium bearing steel, *Fatigue & Fracture of Engineering Materials & Structure*, 25 (8-9) (2002) 813-822.

[3] S. K. Cheng, S. H. Lee and S. C. Chung, Effect of the peening intensity by shot peening, *Transactions of the KSME(A)*, 25 (10) (2001) 1590-1596.

[4] P. Zhang and J. Lindemann, Influence of shot peening on high cycle fatigue properties of the high-strength wrought magnesium alloy AZ80, *ScriptaMaterialia*, 52 (6) (2005) 485-490.

[5] S M. A. S. Torres and H. J. C. Voorwald, An evaluation of shot peening, residual stress and stress relaxation on the fatigue life of AISI 4340 steel, *International Journal of Fatigue*, 24 (8) (2002) 877-886.

[6] Y. Murakami, *Metal fatigue: Effects of small defects and non-metallic inclusions*, First ed. Elsevier Science Ltd, UK (2002).

[7] JIS Z 2274, Method of rotating bending fatigue testing of metals.

[8] ASTM, 1994, Standard test method for determining the effective elastic parameter for X-ray diffraction measurement of residual stress, *ASTM E,*1426 (94) (1994) 932-935.

[9] KS B ISO 1143, Metallic materials - Rotating bar bending fatigue testing.

[10] W. Li, T. Sakai, Q. Li, L.T. Lu and P. Wang, Reliability evaluation on very high cycle fatigue property of GCr15 bearing steel, *International Journal of Fatigue*, 32 (7) (2010) 1096-1107.

[11] J. Y. Lee, D. W. Jung and N. S. Choi, Fatigue fracture behavior and statistical life evaluation of hybrid composite/metal beam-joints for a low-floor bus, *Journal of Composite Materials*, 46 (2011) on-line first.

[12] D. C. Park, 2001, *Electrical engineering probability*, Intervision, Korea.

[13] T. Sakai, Y. Satoand and N. Oguma, Characteristic S-N properties of high-carbon-chromium-bearing steel under axial loading in long-life fatigue, F*atigue & Fracture of Engineering Materials & Structures*, 25 (8-9) (2002) 765-773.

[14] Y. Furuya, S. Matsuoka, T. Abe and K. Yamaguchi, Gigacycle fatigue properties for high-strength low-alloy steel at 100 Hz, 600 Hz, and 20 kHz, *Scripta Materialia*, 46 (2002) 157-162.

Sang-Jae Yoon received his Master's degree from the Department of Mechanical Engineering, Hanyang University, Korea, 2011. His research interests are fatigue fracture and material design.

Nak-Sam Choi received his Ph.D. from Kyushu University, Japan, 1990. He is currently a full professor in the Department of Mechanical Engineering, Hanyang University, Korea. His research interests include the fatigue behavior of materials and composites, acoustic emission analysis, experimental methods for composites and reliability analysis.